2023년 2월

박사학위 논문

Biomechanical Investigation to Establish Stable Fixation Strategies for Distal Tibial Fractures in Various Situations : Finite Element Analysis Studies

조 선 대 학 교 대 학 원

의 학 과

양 성 훈

Biomechanical Investigation to Establish Stable Fixation Strategies for Distal Tibial Fractures in Various Situations : Finite Element Analysis Studies

다양한 상황에서의 원위 경골 골절에 대한 안정적 고정 전략 수립을 위한 생역학적 측정: 유한 요소 해석 연구

2023년 2월 24일

조 선 대 학 교 대 학 원

의 학 과

양 성 훈

Biomechanical Investigation to Establish Stable Fixation Strategies for Distal Tibial Fractures in Various Situations : Finite Element Analysis Studies

지도교수 이 준 영

이 논문을 의학 박사학위신청 논문으로 제출함

2022년 10월

조 선 대 학 교 대 학 원

의 학 과

양 성 훈

양성훈의 박사학위 논문을 인준함

위원장 조선대학교 교수 손 홍 문 (인)

위 원 경상대학교 교수 정 구 희 (인)

위 원 조선대학교 교수 이 광 철 (인)

위 원 조선대학교 교수 조 용 진 (인)

위 원 조선대학교 교수 이 준 영 (인)

2023년 1월

조 선 대 학 교 대 학 원

CONTENTS

LIST OF FIGURES

ABSTRACT

다양한 상황에서의 원위 경골 골절에 대한 안정적 고정 전략 수립을 위한 생역학적 측정; 유한 요소 해석 연구

양 성 훈

지도교수 : 이 준 영

조선대학교 대학원 의학과

목적: 원위 경골 골절 치료에서 골수강 내 금속정과 원위 경골 금속판에서 적절한 내고정물을 선택하는 것은 아주 중요한 부분이지만 아시아인에 대한 원위 경골의 해부학 및 원위 경골 금속판 모양과의 일치성에 대한 연구와 금속판과 금속정 사이의 생역학적 차이를 비교한 연구는 없다. 본 연구는 3D 재건술을 통하여 아시아인의 원위 경골의 해부학적 요소를 파악하고, 원위 경골 금속판과 원위 경골의 일치 정도를 파악하고자 하였습니다. 또한 유한 요소 해석을 통해 원위 경골 골절을 위한 다양한 고정 방법의 구조적 강도를 분석함으로써 임상적 의의를 얻고자 하였다.

대상 및 방법: 경골의 3D 재건술을 위해 IRB 승인 이후 후향적으로 경골 골절이 있었던 19세 이상의 환자를 대상으로 양측 경골 CT 촬영을 한 총 77명의 환자를 대상으로 하였다. 대상들의 수상하지 않은 반대쪽 경골 CT 데이터로 Mimics® 프로그램을 이용하여 3D 경골 모델을 재건하였다. 금속판의 3D모델을 제작하고 원위 경골의 내측에 가상으로 위치시켜 기존의 원위 경골 금속판의 모양과 경골 사

이의 일치 정도를 확인하였다. 원위 경골의 해부학적 특성을 확인하기 위해 Mimics® 프로그램을 사용하여 아시아인의 원위 경골의 뒤틀림 정도와 원위 경골의 오목함의 정도를 파악하였다. 2개의 선을 경골 간부와 원위 경골에 설정한 후 이 두 선 사이의 각도를 측정하여 원위 경골의 뒤틀림 정도를 확인하였다. 원위 경골 내측면에 3개의 점을 경골 간부, 족관절 내과, 그리고 이 두 점 사이 같은 거리에 있는 점을 설정하여 이 3개의 점을 이어 원을 그리고, 원의 지름을 측정하여 원위 경골 내측부의 오목한 정도를 파악하였다. 좌측 경골(SAWBONES®)에 대해 금속정과 금속판을 가장 이상적인 곳에 위치시킨 후 원위 경골에 20mm와 120mm의 결손으로 원위 경골 골절 모델을 만들었다. 20mm 및 120mm 결손에서 금속정 고정술을 시행하였으며 원위 고정의 구성은 2개 및 3개의 교합나사를 삽입한 모델 그리고 2개의 교합 나사 및 차단나사를 삽입한 모델을 만들었다. 금속판 고정술은 20mm결손에 대해서만 시행하였다. Ansys®를 이용한 하중 부하 모델 구축에서 외다리 서기를 구현하기 위해 축성 800N를 내측에 60%, 외측에 40%를 부하 하였으며, 임플란트와 뼈는 직접 접촉된 것으로 가정하였고 제조사에서 제시된 물성치를 적용하였다. 골절 부위의 변형 정도(mm)와 경골 및 임플란트에 발생하는 응력(von Mises stress, VMS, MPa)를 측정하였다.

결과: 원위 경골의 뒤틀린 정도는 평균값 30.06도 (표준편차: 6.50°), 원위 경골의 굴곡 정도는 굴곡선의 지름 평균값이 436.46mm (표준편차: 67.62mm) 확인되었다. 원위 경골의 뒤틀림 정도는 원위 경골의 굴곡 정도와 통계적으로 유의한 관계를 보였다. ($p=0.039$) 원위 경골과 원위 경골 금속판사이의 불일치 하는 부위는 경골 골간단에서 골간으로 넘어가는 부위에서 유격이 크게 확인되었으며 금속판의 모양에 따라 수술적 정복시 경골의 내반 변형 및 외회전 변형이 일어날 수 있음을 확인 하였습니다. 금속정 모델에서 경골 및 내고정물의 응력 분포는 첫번째 교합 나

사 홀 및 주위 내측 피질골에서 최대치를 나타났었으며, 금속판 모델에서는 골절 주위 잠김 홀에서 최대치가 나타났다. 20mm결손 골절의 2개의 교합나사 모델에서 경골의 최대 VMS는 40.35MPa, 3개의 교합나사 모델은 30.12MPa이었으며, 금속판 모델의 유사한 위치에서는 56.39MPa였다. 내고정물의 최대 VMS는 2개의 교합나사 모델에서 251.21MPa, 3개의 교합나사 모델은 202.70MPa이었으며, 금속판 모델의 유사한 위치에서는 510.42 MPa이였다. 120mm 결손 골절의 2개의 교합나사 모델에서 경골의 최대 VMS는 38.86MPa, 3개의 교합나사 모델은 25.30MPa이었으며, 차단나사 모델에서는 25.74MPa이었다. 내고정물의 최대 VMS는 2개의 교합나사 모델에서 243.65MPa, 3개의 교합나사 모델은 198.71MPa이었으며, 차단나사 모델에서는 187.17MPa이었다.

결론: 금속정 고정술에서 원위 골편의 고정력을 유지하기 위해서는 첫번째 교합나사의 최대 고정력을 확보하는 것이 제일 중요하게 되며, 2개의 교합나사 고정술 보다 3개의 교합나사를 이용한 고정술이 생역학적으로 안정적이며 분쇄가 심한 골절에서는 3개의 교합나사 고정술보다 차단 나사못 고정술이 생역학적으로 안정적이었다. 금속판 고정술에서는 골절 주위의 근접 잠김홀 및 피질골에서 최대의 응력이 집중되는 점을 감안하여 최대한의 고정력이 확보될 수 있게 나사못 고정술이 이루어져야 할 것으로 판단된다.

색인단어: 원위 경골, 골절, 내고정술, 유한요소 해석

I. INTRODUCTION

Recently, intramedullary nail (IMN) fixation has evolved for a non-diaphyseal tibial fracture, allowing for early mobilization and reproducible recovery of physical function. However, with the innovative development of locking plate technology, plate fixation is regarded as the current standard of treatment for intra- and extra-articular distal fractures. Concerning anatomic features, from diaphysis to distal metaphysis, the tibia transitions from a triangular to a rounded shape and the medial side for plate fixation has a torsional alignment with concavity because of tibial plafond.[1)] Furthermore, since the soft tissue envelope on the medial side of tibia has no muscular layer, anatomically pre-contoured, angular stable plates for distal tibia (distal tibial plate) usually prominent under the skin can cause soft tissue irritation even if there is a good conformity between them.[2)]

When performing a medial plate fixation for a distal tibial fracture (distal tibial plating), there are two important considerations. First, although available distal tibial plates are well developed based on Caucasian people, anatomical research on the conformity in Asians who have shorter stature and varus tibia has not been performed yet. Through academic communications between orthopaedic surgeons, it is well known that there is a significant inconformity. Thus, intraoperative surgical reduction based on the distal medial plate can cause torsional and varus malalignment. Thus, the optimal position to minimize the gap between plate and tibia might be identified by performing an anatomic study

using Asian tibia. Second, it is necessary to biomechanically determine the difference in fixation strength between IMN and plate fixation. Although a closed reduction is more complex and often technically challenging to achieve appropriate alignment and length, minimally invasive plate osteosynthesis (MIPO) has explosively replaced conventional open plating recently to prevent additional soft tissue damage around the fracture site.

The distal tibia has an increased canal diameter with a thin cortex owing to an hourglass-shape of the medullary canal. Since IMN fixation could not achieve a tight endosteal fit, a distal fixation construct should be maintained with interlocking screws. When performing an IMN fixation for distal tibial fracture (distal tibial nailing), a surgeon must consider several important things: 1) how to achieve functional reduction without causing additional soft tissue damage around fracture site? 2) can interlocking screws provide sufficient fixation strength to distal fragment? 3) are there any biomechanically advantages over MIPO? 4) will additional implants be needed for maintaining reduction of IMN fixation construct? To choose an optimal implant for distal tibial fracture, although related patient's and surgeon's factors need to be considered, biomechanical differences between distal tibial plating and nailing must be identified experimentally.

For these biomechanical purposes, finite element (FE) analysis has received wide acceptance in orthopedic research. It is the preferred method for solving encountered problems in fracture fixation biomechanics by performing strain analysis of bones and load-bearing implants for structure-mechanical issues.[3-5)]

Biomechanical studies via computer simulation allow for a 360° free rotation with magnification in any plane to analyze stress distribution at the fracture or implant site. Therefore, the FE method was used in this study to determine structural-mechanical stabilities of various fixation constructs after simulating a distal tibial fracture. Objectives of this computational study were: (1) to evaluate anatomical features of distal tibia using a 3D tibiofibular model at actual size, (2) to assess plate conformity by virtual fixation, (3) to investigate biomechanical stiffness of plate fixation constructs, (4) to assess biomechanical differences according to screw configuration of IMN fixation, and (5) to introduce clinical implications.

II. MATERIALS AND METHODS

1. Subjects' Data Collection

The ethics committee of institution approved the study protocol (GNUCH-F***19-003-01) and medical records and radiographs of tibial fractures were retrospectively analyzed. In the present study, subjects with tibia fracture were reviewed and patients aged above 19 years were included. Based on medical history review and radiographs taken at the time of injury, patients with metastatic bone tumor, osteomyelitis, lower leg deformity, or joint problems were excluded. CT scanning of subjects should be performed from knee to ankle joint for achieving the entire length of both tibias. Finally, 77 patients (51 males and 26 females) with a tibia fracture who underwent CT scanning for both legs were enrolled in this study. The average age of all patients was 47.9 years (range, 19-82 years) and the average length of tibia was 35.77 cm (range, 29.00-40.6 cm).

2. 3D modeling of implant

For FE analysis, ZNN® (Zimmer Natural Nail® System-Tibia, Zimmer Biomet, Warsaw, IN, USA) and distal tibial plate (distal medial tibial plate®, DePuy-Synthes, Oberdorf, Switzerland) were created using a 3D computer-aided design (CAD) software of SolidWorks 2021® (Dassault Systems SolidWorks Co, MA, USA). For virtual fixation of distal tibia, three models of distal tibial plate (two plates of DePuy-Synthes, one plate of Zimmer) in STL format were created using a 3D sensor (Comet5®; Carl Zeiss, Steinbichler, Germany) at actual size.

3. Development of 3D Asian tibiofibular model at actual size

CT data of tibial fractures were imported into Mimics® software (Materialise Interactive Medical Image Control System; Materialise, Antwerp, Belgium). The non-injured tibia on the opposite side was selected as a cropping area to reconstruct 3D models of Asian tibia and fibula with the medullary canal. Talus and distal femur were removed to facilitate 3D rendering. Using mimics® software, a 3D Asian tibiofibular model at actual size could allow free 360° rotations with magnification in any plane to virtually place a distal tibial plate in the optimal position (Fig. 1).

4. Development of 3D tibia and tibiofibular models for FEA

We used a commercially available CAD three-dimensional (3D) image file of a standard fourth-generation composite left tibia and fibula bone model (SAWBONES®, Vashon, WA, USA). For making the tibiofibular model, 3D CAD models of tibia and fibula were imported into 3D-Matics® software (Materialise Interactive Medical Image Control System; Materialise, Antwerp, Belgium). Ideal reduction and symmetric congruency of distal tibiofibular syndesmosis were simulated using moving tools of the 3D-Matics® software. Definitive position of the fibula and reduction adequacy of ankle mortise were fine-tuned and verified by an experienced surgeon. Finally, syndesmotic ligaments (20 mm in width and 2 mm in thickness) including the anteroinferior tibiofibular ligament, posteroinferior tibiofibular ligament, and interosseous ligament were created and placed in their anatomical positions (Fig. 2).

5. Computational simulation of distal tibial plating

After obtaining 3D models of implants and bones, the distal tibial plate was virtually placed and aligned on the medial side using moving tools of Mimics® software. The method followed was used to minimize the gap and to maximize the conformity with bone in concordance with the well-accepted technique (Fig. 3).

6. Computational simulation of distal tibial fracture

Based on the definition of distal tibial metaphysis which construct a square, with the sides of length[1,6], a distal tibial fracture was made parallel to 50 mm above the distal articular surface. For simulating the bony comminution and wedge fragments not supported by screws, bone loss of the distal tibial shaft was created and regarded as anatomically reduced.

7. 3D modeling for FE analysis

3D models of implant and bones were imported to ANSYS® software (Ansys 19.0, Ansys Inc., Canonsburg, PA, USA) for establishing an FE model by remeshing. We used the following principles for fixation constructs: 1) based on the fixed angle of locking hole, we determined screw trajectory of the distal tibial plate; 2) the contact between plate and screw was designed to simulate the locking head screw (LHS) mechanism; 3) for purchasing the opposite cortex, all screws of plate and IMN protruded over 2 mm. The distal end of the model was

completely fixed with the square structure that followed the shape of the talus to fit the ankle mortise. Assembly models were constructed as follows: (1) distal plating/nailing model without fracture, (2) distal plating/nailing model with bone loss of 20 mm, and (3) distal nailing model with bone loss of 120 mm. Among them, models fixed with IMN were combined according to the configuration of distal screw fixation: 1st mediolateral (ML) interlocking screw, 2nd anteroposterior (AP) interlocking screw, 3rd ML interlocking screw, and blocking screw (Fig. 4).

According to the well-established and approved test contact setup method described in previous studies. An axial force of 800 N with a distribution of 60% to the medial compartment and 40% to the lateral compartment was applied to simulate the load on the knee of an adult during a single limb stance.[7,8] Axial compressive load was applied using two cylinders. Proximal portions of models were removed to eliminate stress distribution of tibia and fibula. We could not evaluate torsional results in these models.

8. Material properties, loading conditions, and boundary conditions

We assigned material properties of synthetic tibia and fibula in accordance with the manufacturer's specifications for fourth generation Sawbones. The Young's modulus of a cortical bone was set to 7,200 MPa with a Poisson's ratio (y) of 0.350. The Young's modulus (135 megapascals, MPa) and Poisson's ratio (y) were set to 0.225 for a cancellous bone. The density was 1.5 g/cm^3 for a cortical bone and 0.2 g/cm^3 for a cancellous bone.[9,10] This study assumed that all metals in implants had homogeneous, isotropic, and elastic properties of

titanium alloy. The Young's modulus of titanium alloy was set at 96,000 MPa with a Poisson's ratio (y) of 0.36 and an implant density of 4.62 g/cm^3. Structural steel had a Young's modulus of 200,000 MPa and a Poisson's radio of 0.3.[9)]

The implant was in direct contact with the bone. Interactions between surfaces of plates or nails, screws, and bone were defined as follows: 1) locking screw threaded connections with plate were assumed as fully bonded; 2) the plate and IMN could slide between fragments with bone during mechanical loading;[11,12)] 3) the screw connection with cortical bone was bonded; and 4) the connection between interlocking screws and the hole of IMN was modeled with sliding contact.[11)] We performed finite element analysis using commercially available Ansys® software and VMS (von Mises stress) measured in MPa with fracture displacement of the implant relative to the bone (as a measure of relative fixation strength).

9. Anatomical analysis of distal tibia

When using the Mimics® software to measure 3D distal torsion at actual size, two reference lines were virtually placed and aligned on the medial surface of the middle shaft and the distal metaphysis. 3D tibia models were then imported to into 3D-Matics® software and converted into 2D axial models to eliminate projection error of tibial torsion. The acute angle form by the two reference lines was measured as distal tibial torsion (Fig. 5). Next, measurement tools within the Mimics® software were used to provide a reliable selection of points. Three points on the medial surface of distal tibia surface were marked (point A was

located at the midshaft, point C was located 2 cm in the medial malleolus, and point B was equidistant between points A and C). According to these three points, the diameter of curve (DOC) of distal medial surface was measured (Fig. 6). Finally, definitive positions of all measurement tools were fine-tuned and verified by an experienced surgeon.

10. Validation and outcome measures of FE analysis

The validation was supported through comparison of global axial stiffness to literature-reported values from a study with similar loads and boundary conditions having small differences in implant geometry.[13] Soft tissues of muscle and ligament forces were not used in these simulations because ankle joint structure of articular cartilage and syndesmotic joint could not be applied. Computational model outputs included the maximum VMS for interlocking screw hole, the locking screw hole, and the tibial cortex of the distal fixation construct.

11. Statistical method

Numerical data are presented as mean and range or mean and standard deviation. Statistical significance was set at $p < 0.05$. All statistical analyses were performed using SPSS statistical software package for Windows (version 20.0; SPSS, Chicago, IL, USA).

III. RESULTS

1. Distal tibial torsion and plate conformity

As is already well-known, we could clearly demonstrate that the tibial shaft transitioned from a triangular to a rounded shape and the anterior border of diaphysis twisted anteromedially from the diaphysis to the distal metaphysis. The average length of the tibia was 35.77 cm (range, 29.00-40.6 cm, SD: 2.57cm). The distal torsion had an average value of 30.06° (range, 12.74-48.76°, SD: 6.50°). Distal DOC had an average value of 436.46 mm (range, 287.52-436.46 mm, SD: 67.62 mm). By independent samples T-test, sex had no statistical significance on distal torsion (p = 0.425) or distal DOC (p = 0.114). Distal torsion was statistically correlated with distal DOC (p = 0.039) but not with tibial length (p = 0.989).

In the computational simulation of distal tibial plating, the mismatch between tibia and implant was prominent in the meta-diaphyseal junction area in which fractures commonly occurred. By moving the plate anteriorly, the gap was increased in the distal diaphysis and the mismatch could be clearly visualized in the internally rotational view (Fig. 7). If the reduction was achieved based on plate conformity, the varus and external rotation deformity might occur. By moving the plate posterior along the posterior border, the mismatch was prominent in the tibial shaft with significant rotational malalignment internally because of distal tibial torsion (Fig. 7).

2. FE analysis of distal tibial nailing & plating without fracture

The assembled tibia model without fracture had the maximum displacement occurring at the upper part of tibia as shown in Fig. 8. Total displacement was 3.00 mm for the two-screw model, 4.17 mm for the three-screw model, and 4.75 mm for the plating model (Fig. 9). VMS distributions for tibia were assessed. Results are shown in Fig. 10. Stress distribution areas had maximum VMS values at the lateral cortex around the 1st interlocking screw for IMN models and the medial cortex of most proximal hole for plate models. The maximum VMS at the lateral cortex around the 1st interlocking screw was 19.12 MPa for the two-screw model and 14.94 MPa for the three-screw model. In the area similar to the IMN model, the VMS value was 9.56 MPa (Fig 11). VMS distributions for distal fixation constructs were assessed. Results are shown in Fig. 12. Stress distribution areas had the maximum VMS values at the 1st hole of the interlocking screw for IMN models and at the 3rd locking hole from the distal end for plate models. The maximum VMS value was 84.01 MPa for the two-screw model, 65.97 MPa for the three-screw model, and 97.03 MPa for the plating model. However, in an area similar to the 1st hole of the IMN model, the VMS value of the 5th locking hole was 61.03 MPa (Fig. 13).

3. FE analysis of distal tibial nailing & plating with bone loss of 20 mm

The assembled tibia model without bone loss of 20 mm had the maximum displacement occurring at the upper part of the tibia as shown in Fig. 14. Total displacement was 6.13 mm for the two-screw model, 6.19 mm for the three-

screw model, and 17.07 mm for the plating model (Fig. 15). VMS distributions for tibia were assessed. Results are shown in Fig. 16. Stress distribution areas had the maximum VMS values at the medial cortex around the 1st interlocking screw in IMN models and the medial cortex of just the proximal hole above the fracture in the plating model. The maximum VMS at the medial cortex around the 1st interlocking screw was 40.35 MPa for the two-screw model and 30.12 MPa for the three-screw model. In the area similar to the IMN model, the VMS value was 56.39 MPa (Fig. 17). VMS distributions for distal fixation constructs were assessed. Results are shown in Fig. 18. Stress distribution areas had the maximum VMS values at the 1st hole of the interlocking screw in IMN models and the 5th locking hole just below the fracture site in the plating model. The maximum VMS value was 251.21 MPa for the two-screw model, 202.70 MPa for the three-screw model, and 510.42 MPa for the plate model (Fig. 19).

5. FE analysis of distal tibial nailing with bone loss of 120 mm

The assembled tibia model without bone loss of 120 mm showed the maximum displacement occurring at the upper part of the tibia as shown in Fig. 20. The total displacement was 7.88 mm for the two-screw model, 8.27 mm for the three-screw model, and 7.78 mm for the blocking screw model (Fig. 21). VMS distributions for tibia were assessed. Results are shown in Fig. 22. Stress distribution areas had the maximum VMS values at the medial cortex around the 1st interlocking screw in IMN models. The maximum VMS at the medial cortex around the 1st interlocking screw was 38.86 MPa for the two-screw model, 25.30

MPa for the three-screw model, and 25.74 MPa for the blocking screw model (Fig. 23). VMS distributions for distal fixation constructs were assessed. Results are shown in Fig. 24. Stress distribution areas in IMN models had the maximum VMS values at the 1st hole of the interlocking screw. The maximum VMS value was 243.65 MPa for the two-screw model, 198.71 MPa for the three-screw model, and 187.17 MPa for the blocking screw model (Fig. 25).

6. FE analysis of 3D tibiofibular fracture model with bone loss of 20mm

VMS distributions for tibiofibular model were assessed. Results are shown in Fig. 26. Stress distribution areas had the maximum VMS values at the medial cortex around the 1st interlocking screw in both the tibia model and the tibiofibular model. The maximum VMS of tibiofibular model was 42.11 MPa for the two-screw model and 27.80 MPa for the three-screw model (Fig. 26). VMS distributions for distal fixation construct were assessed. Results are shown in Fig. 27. Stress distribution areas had the maximum VMS values at the 1st hole for the interlocking screw both in the tibia model and the tibiofibular model. The maximum VMS of tibiofibular model was 253.29 MPa for the two-screw model and 201.14 MPa for the three-screw model (Fig. 27). Although there was no significant VMS difference, the tibiofibular model had slightly less VMS values than the tibia model in the distal tibia and distal fixation construct.

IV. DISCUSSION

Managing distal tibia fractures is crucial to decide between distal tibial nailing and plating. Although distal tibial plating has been increasingly performed with popularization of bridge plating based on the locking plate technology, distal tibial nailing provides several advantages including biomechanically load-sharing function, minimal violation of soft tissue envelope, and less space-occupying effect.[1,14] Although surgeons might consider many factors including fracture characteristics, soft tissue conditions, and others, biomechanical stability of the distal fixation construct should be a prerequisite for implant choice. Therefore, this present study was conducted to determine structural-mechanical stabilities of various distal fixation constructs through FE analysis following simulation of a distal tibia fracture with comminuted zone and wedge fragments not supported by screws. This computational analysis enabled us to demonstrate several interesting findings. First, the plating model of 20 mm-gap had significantly increased deformation and much different stress distribution of the tibia and distal fixation construct compared with the IMN model of 20 mm-gap (Fig. 28). Concerning stress distributions of IMN models, the distal tibia and distal fixation construct had the maximal VMS value at the medial cortex around the 1st interlocking screw and at the 1st interlocking screw hole, respectively. Thus, a fully osseous purchase of the 1st interlocking screw might be a perquisite for achieving the optimal strength of IMN. Concerning stress distributions of plating models, the distal tibia and the distal fixation construct had the maximal VMS

value at the medial cortex of just the proximal hole above the fracture and at the locking hole just below the fracture site, respectively. These results indicate that two locking screws around the fracture site are important for maintaining the fixation construct. Thus, they should be fully purchased to the lateral cortex and placed as close as possible when considering distal plating. Furthermore, in distal tibial plating through bridge plating, two locking screws should be placed as close as possible to the fracture site.

Second, for distal tibia fracture model of 120 mm-gap, we did not create a plating model because this construct was inappropriate for fracture with a significant gap. Practically, in this situation, surgeons must decide the distal fixation constructs by combining interlocking screws and blocking screws. In this experiment, we created three models (two-screw, three-screw, and blocking screw models) with the 2nd AP interlocking screw replaced. Among fixation constructs of 120 mm-gap, the blocking screw models had the least deformation. Thus, they were stiffer than three-screw models. Concerning stress distributions of assembled models, the VMS distribution for an implant is an indicator of the yielding of metals. It can be explained by the mechanics of load sharing.[15] When a blocking screw model was compared with a three-screw model, the maximal VMS value of implant was decreased in the 1st interlocking screw hole. Considering that a higher stress value of an implant will lead to a higher possibility of implant failure, the IMN fixation strategy for distal tibial fracture with significant bone loss might be that the blocking screw technique is better than a three-screw technique. However, to maintain consistency of the 1st interlocking

screw fixation, we did not create additional combinations of blocking screws such as substitution of 1st ML interlocking screw or 3rd ML interlocking screw. In the future, changes of biomechanical strength according to the location of the blocking screw should be studied.

Third, for constructing 3D tibiofibular models of distal fixation construct, we used a commercially available CAD 3D model because material properties could be obtained from manufacturer's specifications. When a tibia model was compared with a tibiofibular model, the tibiofibular model had slightly less VMS values both in the distal tibia and the distal fixation construct. Therefore, although the importance of fibular fracture was already proven and clinically known, we were able to confirm the usefulness of this tibiofibular model once again. However, we could not create a fibular fracture or plate fixation owing to technical difficulties and inconsistency of FE analysis.

Fourth, through our computational simulation study for distal tibial torsion, we could provide Asian data that the distal torsion had an average value of 30.06 ± 6.50° and the distal DOC had an average value of 436.46 ± 67.62 mm. Interestingly, the distal torsion was statistically correlated with distal DOC (p = 0.039) but not with tibial length (p = 0.989). Concerning that Asians have short stature and varus tibia, the distal tibial torsion might be prominent compared with Caucasians. Thus, our findings are valuable for understanding 3D morphologic features of distal tibia. They could be used to modify pre- or intra-operative bending and torsion of a distal tibial plate. Furthermore, a new and innovative implant for Asian distal tibia that could increase tibial torsion and mediolateral

angle should be designed.

Despite these interesting findings, this biomechanical study has several limitations. First, we simulated a highly simplified model in a digital tibia without a soft tissue envelope. Second, our results had rather descriptive characters because the distal tibial fracture was perfectly reduced with gap. Third, the friction between implant and bone could not be considered because of technical difficulties. Nevertheless, our FE analysis could evaluate structure-mechanical strength, VMS distribution in the tibia, and implant under the same conditions. Although implant choice should be determined according to the degree of displacement, fracture type, physiological age, and bone quality, our results may directly suggest technical relevance of maximizing structural strength and minimizing fixation failure. Although biomechanical testing with cadavers remains the “gold standard” for providing the primary stability assessment of fracture fixation constructs, this 3D modeling to establish stable fixation strategies for distal tibial fractures can be tested in silico. Therefore, in the future, we could conduct additional experiments and change numerical parameters including implant position, implant type, fracture characteristics, and fixation constructs without the need to construct a new model.

V. CONCLUSION

For maintaining distal fracture fixation, it is most important to achieve full purchase of 1st interlocking screw in IMN and just above the locking hole of the fracture in plating. In an IMN fixation, the three-screw model was more biomechanically stable than the two-screw model and the blocking screw model had more structural stability than the three-screw model. Considering stress distribution of implant and tibia, in case of fracture comminution, the IMN model was more stable than the plating model and the three-screw model was better than the two-screw model. Furthermore, in case of extensive comminution, the IMN model of blocking screw fixation might be biomechanically superior to the three-screw model because there was less deformation of fixation construct with less stress around the 1st interlocking screw hole.

REFERENCES

1. Bedi A, Le TT, Karunakar MA. Surgical treatment of nonarticular distal tibia fractures. J Am Acad Orthop Surg. 2006;14:406-16.

2. Kuhn S, Greenfield J, Arand C, et al. Treatment of distal intraarticular tibial fractures: A biomechanical evaluation of intramedullary nailing vs. angle-stable plate osteosynthesis. Injury. 2015;46:S99-S103.

3. Kluess D. Finite element analysis in orthopaedic biomechanics. Citeseer: 2010.

4. Kwak DK, Kim WH, Lee SJ, Rhyu SH, Jang CY, Yoo JH. Biomechanical Comparison of Three Different Intramedullary Nails for Fixation of Unstable Basicervical Intertrochanteric Fractures of the Proximal Femur: Experimental Studies. Biomed Res Int. 2018;2018:7618079.

5. Dragomir-Daescu D, Salas C, Uthamaraj S, Rossman T. Quantitative computed tomography-based finite element analysis predictions of femoral strength and stiffness depend on computed tomography settings. J Biomech. 2015;48:153-61.

6. Robinson CM, McLauchlan GJ, McLean IP, CM C-B. Distal metaphyseal fractures of the tibia with minimal involvement of the ankle. Classification and treatment by locked intramedullary nailing. J Bone Joint Surg Br. 1995;77:781-7.

7. Raja Izaham RM, Abdul Kadir MR, Abdul Rashid AH, Hossain MG, Kamarul T. Finite element analysis of Puddu and Tomofix plate fixation for open wedge high tibial osteotomy. Injury. 2012;43:898-902.

8. Sonoda N, Chosa E, Totoribe K, Tajima N. Biomechanical analysis for stress fractures of the anterior middle third of the tibia in athletes: nonlinear analysis

using a three-dimensional finite element method. J Orthop Sci. 2003;8:505-13.

9. Song Z, Wang Q, Ma T, et al. Failure analysis of primary surgery and therapeutic strategy of revision surgery for complex tibial plateau fractures. J Orthop Surg Res. 2019;14:110.

10. Bernard S, Schneider J, Varga P, Laugier P, Raum K, Grimal Q. Elasticity-density and viscoelasticity-density relationships at the tibia mid-diaphysis assessed from resonant ultrasound spectroscopy measurements. Biomech Model Mechanobiol. 2016;15:97-109.

11. Tucker SM, Wee H, Fox E, Reid JS, Lewis GS. Parametric finite element analysis of intramedullary nail fixation of proximal femur fractures. J Orthop Res. 2019;37:2358-66.

12. Lewis GS, Mischler D, Wee H, Reid JS, Varga P. Finite element analysis of fracture fixation. Curr Osteoporos Rep. 2021;19:403-16.

13. Santolini E, West R, Giannoudis PV. Risk factors for long bone fracture non-union: a stratification approach based on the level of the existing scientific evidence. Injury. 2015;46:S8-S19.

14. Costa ML, Achten J, Griffin J, et al. Effect of locking plate fixation vs intramedullary nail fixation on 6-month disability among adults with displaced fracture of the distal tibia: The UK FixDT randomized clinical trial. JAMA. 2017;318:1767-76.

15. Goffin JM, Pankaj P, Simpson AH. The importance of lag screw position for the stabilization of trochanteric fractures with a sliding hip screw: a subject-specific finite element study. J Orthop Res. 2013;31:596-600.

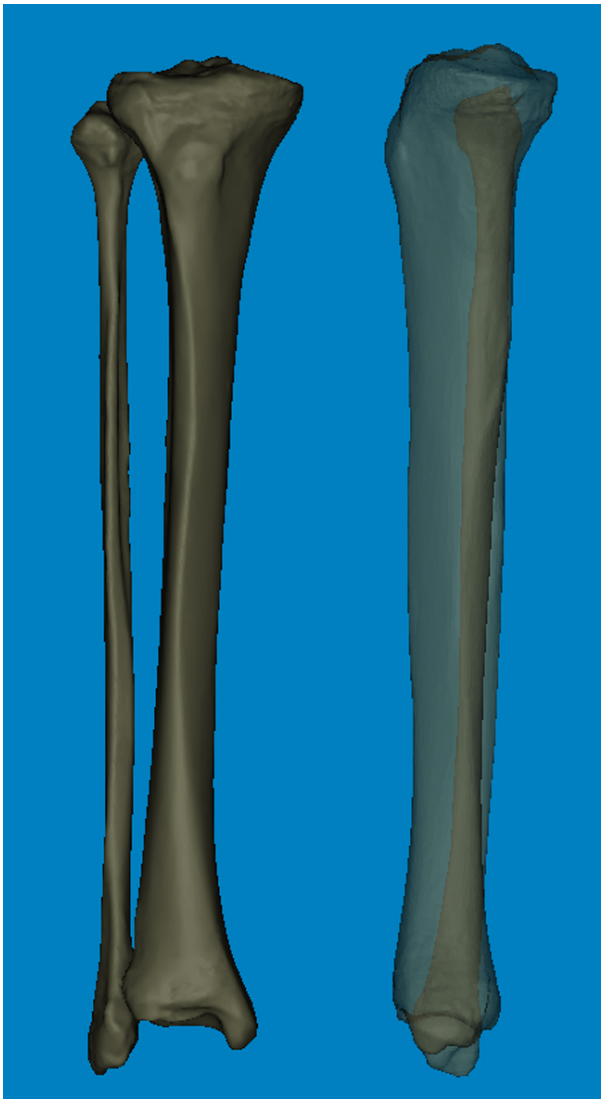

Figure 1. (A) The non-injured tibia on the opposite side was selected as a cropping area to reconstruct 3D models of Asian tibia and fibula with the medullary canal. The talus and distal femur were removed to facilitate the 3D rendering. (B) By using a 3D rendering program (Mimics®), the IMN was virtually placed in the optimal position.

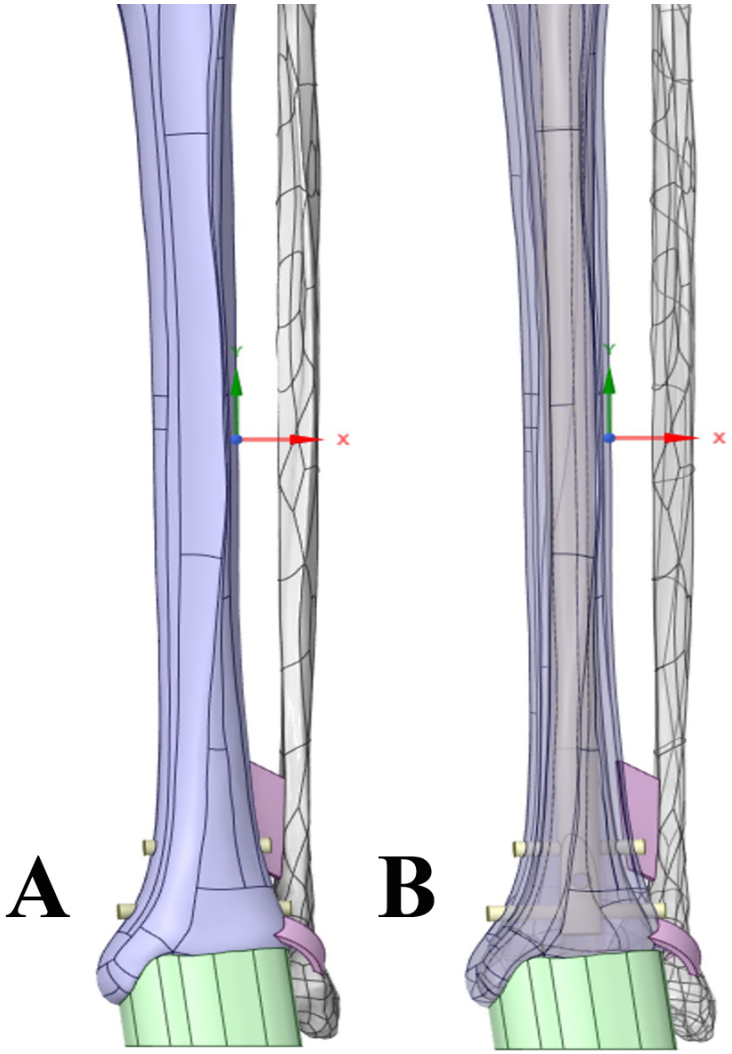

Figure 2. (A, B) The tibiofibular model was created from 3D CAD files, which were imported into 3D-Matics® software. Ideal reduction and symmetric congruency of distal tibiofibular syndesmosis were simulated and syndesmotic ligaments (20 mm in width and 2 mm in thickness) including the anteroinferior tibiofibular ligament, posteroinferior tibiofibular ligament, and interosseous ligament were created in their anatomical positions.

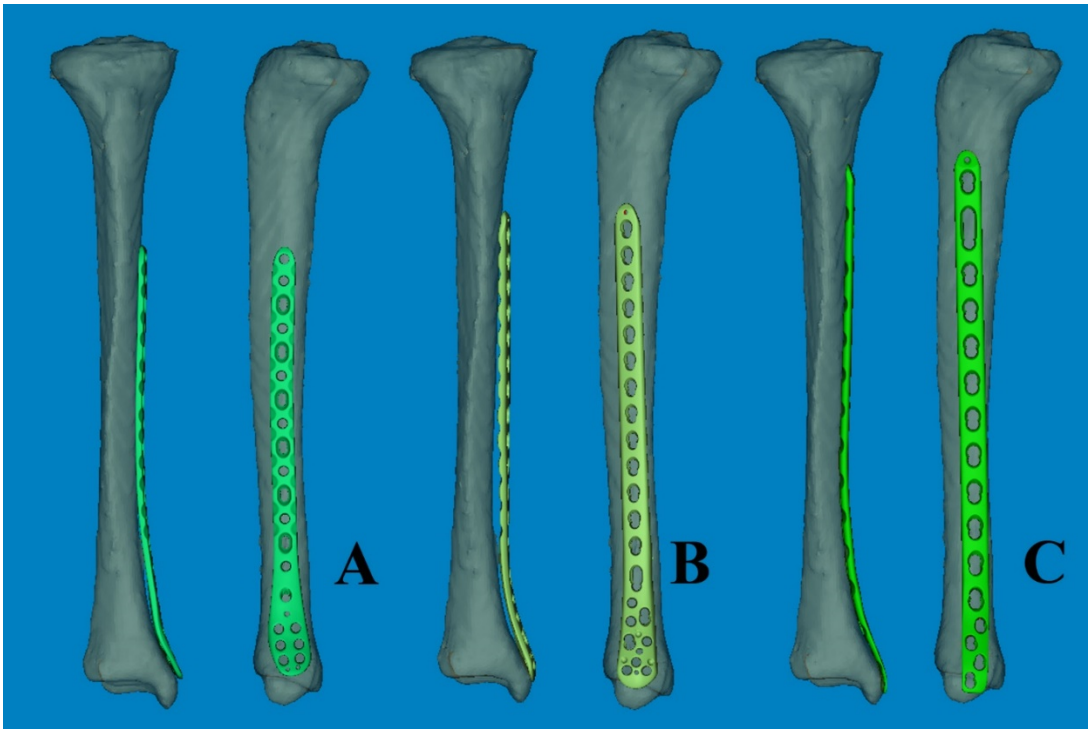

Figure 3. Distal tibial plates were placed in the ideal position. (A) Distal tibial plate of Zimmer, (B, C) Distal tibial plates of Depuy-Synthes.

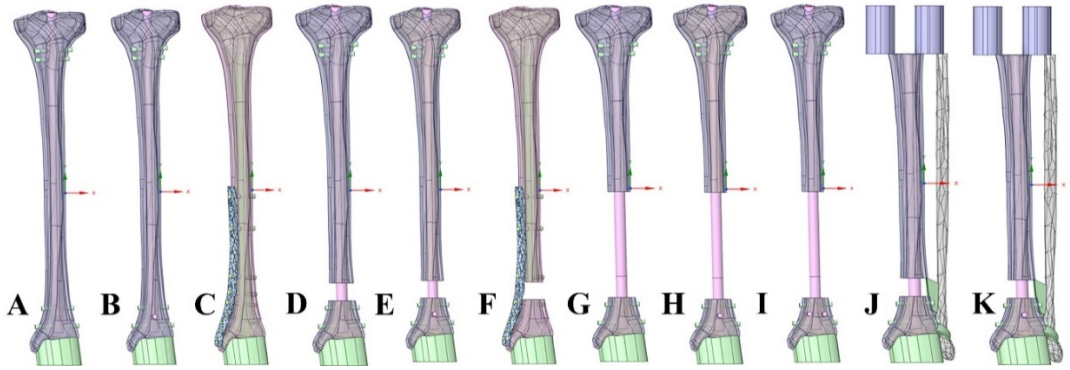

Figure 4. Assembly models were constructed as follows. No tibia fracture group: (A) IMN fixation model of two-screw, (B) three-screw, and (C) Plating model. Tibia 20 mm-gap group: (D) IMN fixation model of two-screw, (E) three-screw, and (F) Plating model. Tibia 120 mm-gap group: (G) IMN fixation model of two-screw, (H) three-screw, and (I) blocking screw model. Tibiofibular 20 mm-gap group: (J) IMN fixation model of two-screw, (K) three-screw model.

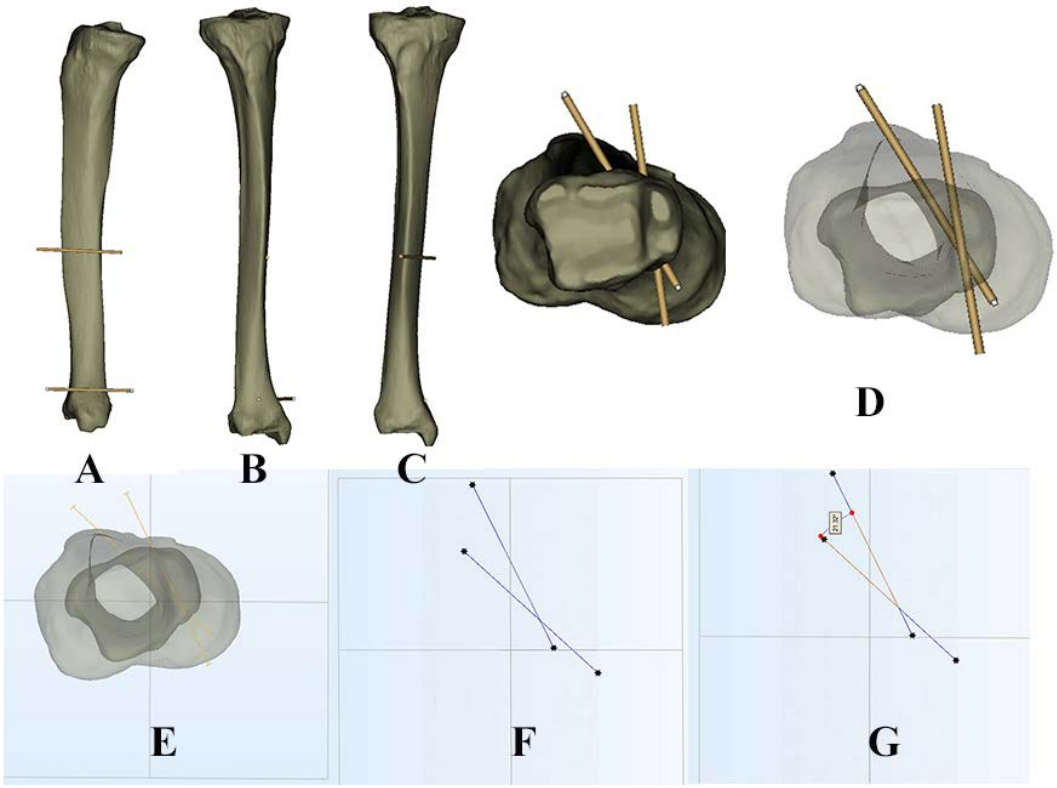

Figure 5. (A,B,C,D) Two reference lines were virtually placed and aligned on the medial surface of middle shaft and distal shaft using the Mimics® software. (E,F,G) Tibia models were converted from 3D models into 2D axial models using the 3D-Matics® software. The acute angle by two reference lines was measured as distal tibial torsion.

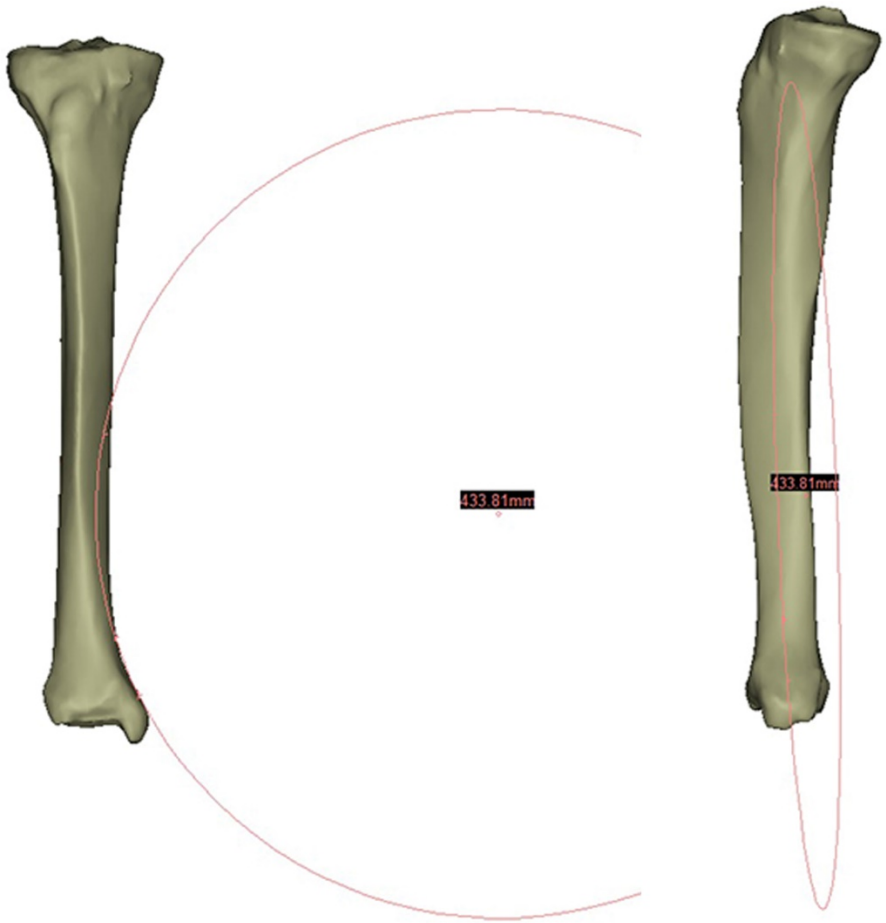

Figure 6. According to these three points, the diameter of curve (DOC) of distal medial surface was measured.

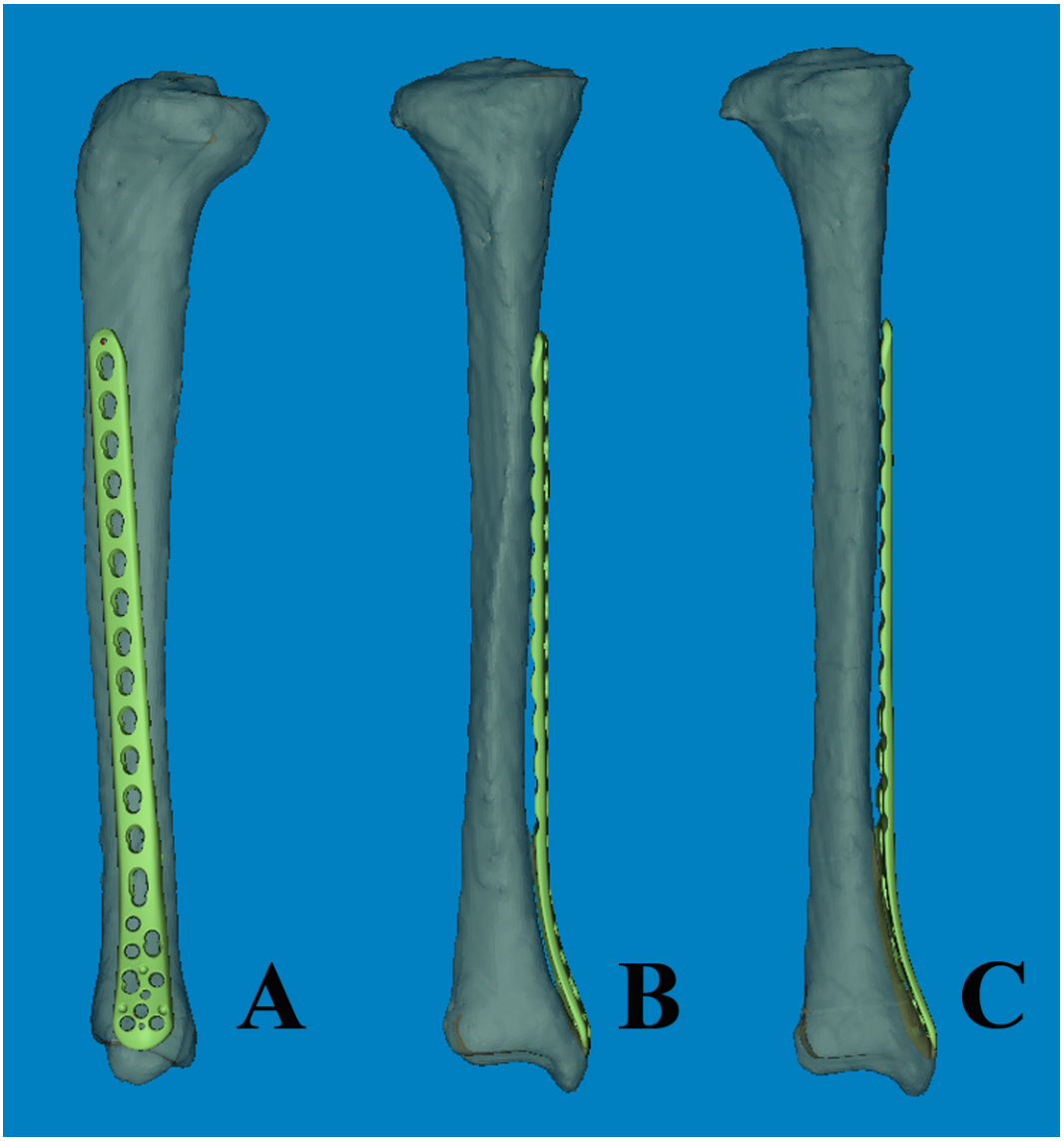

Figure 7. By moving the plate anteriorly, the gap was increased in the distal diaphysis and the mismatch could be clearly visualized in the internally rotational view.

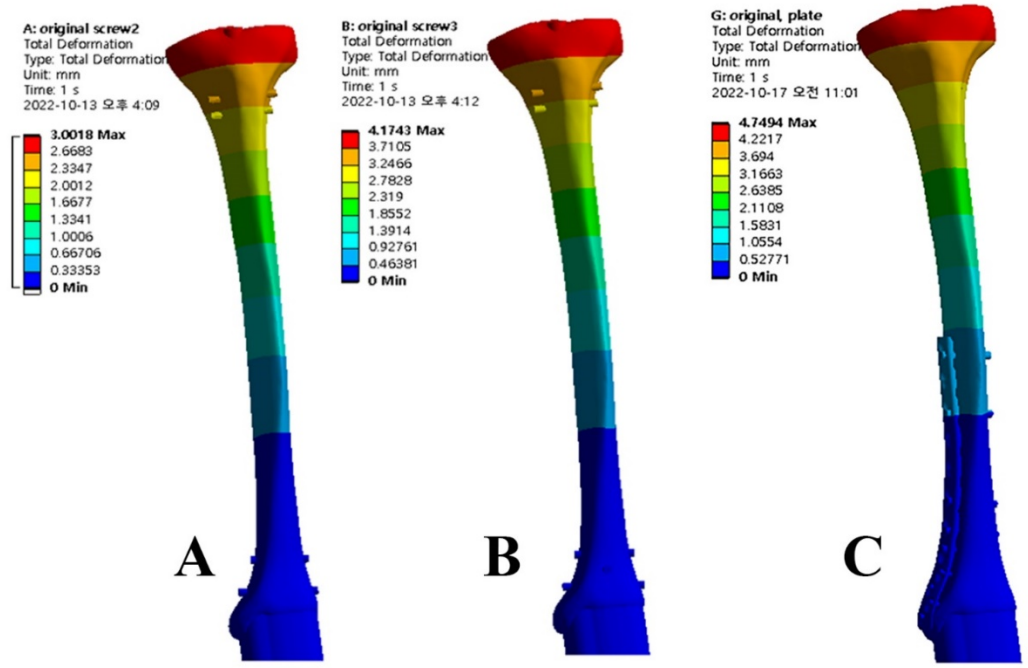

Figure 8. The assembly tibia model without fracture indicates the maximum displacement occurring at the upper part of tibia: (A) IMN of two-screw model, (B) IMN of three-screw model, and (C) Plating model.

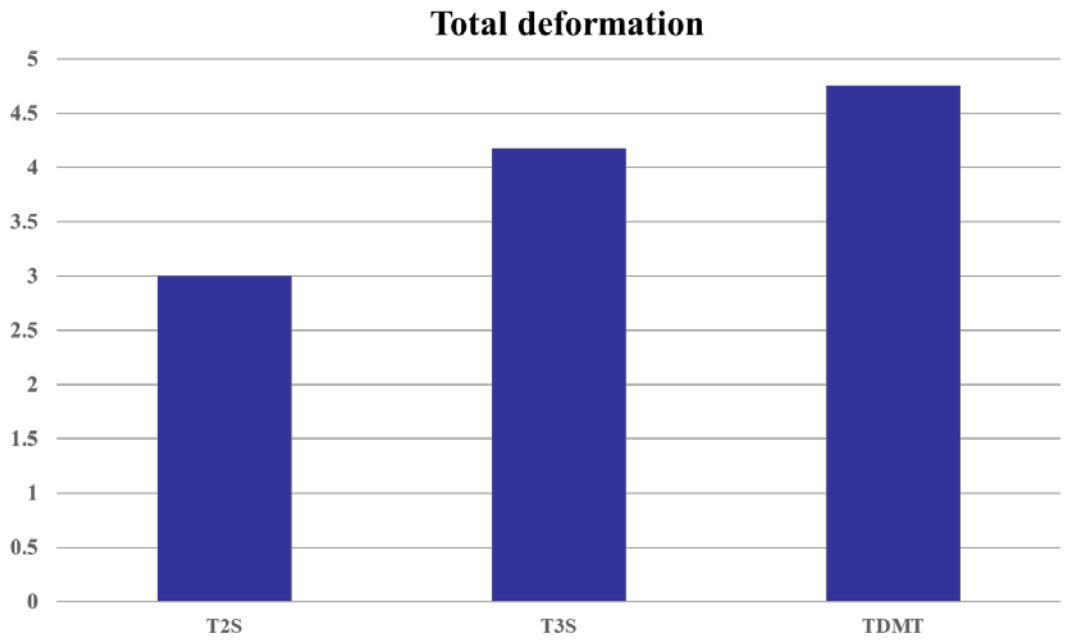

Figure 9. The total displacement was 3.00 mm for the two-screw model, 4.17 mm for the three-screw model, and 4.75 mm for the plating model: (A) IMN of two-screw model (T2S), (B) IMN of three-screw model (T3S), and (C) Plating model (TDMT)

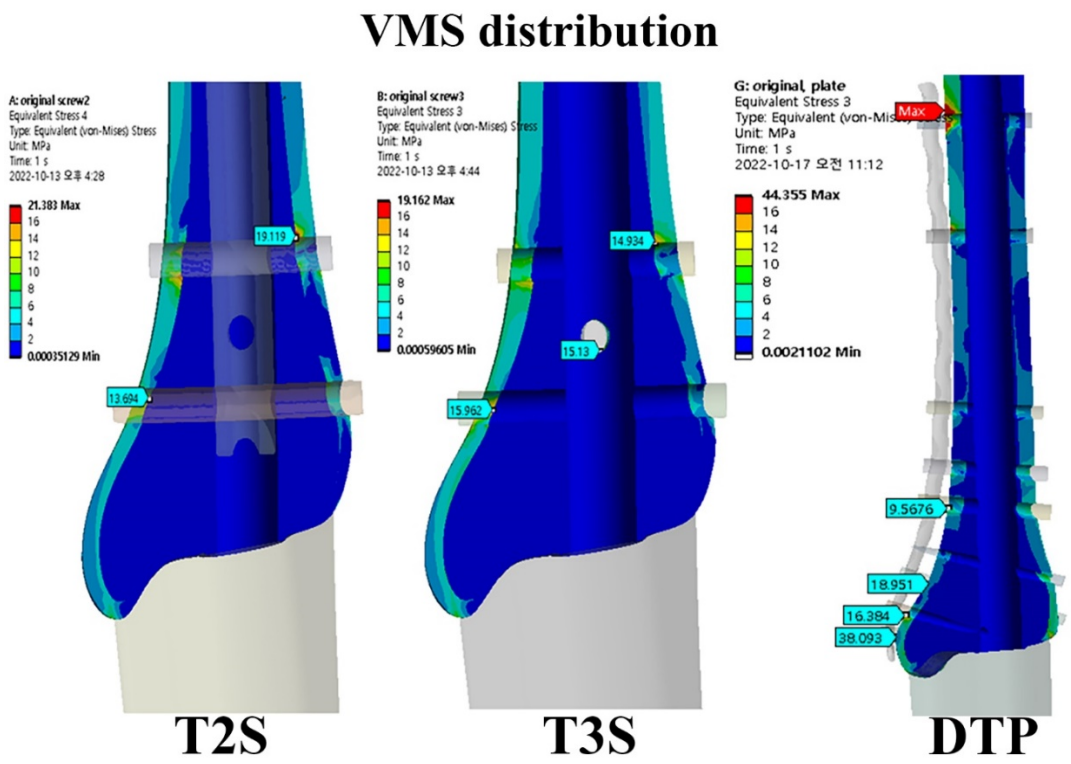

Figure 10. Stress distribution areas had maximum VMS values at the lateral cortex around the 1st interlocking screw in IMN models and at the medial cortex of most proximal hole under the plate in the plating model: (A) IMN of two-screw model (T2S), (B) IMN of three-screw model (T3S), and (C) Plating model (TDMT).

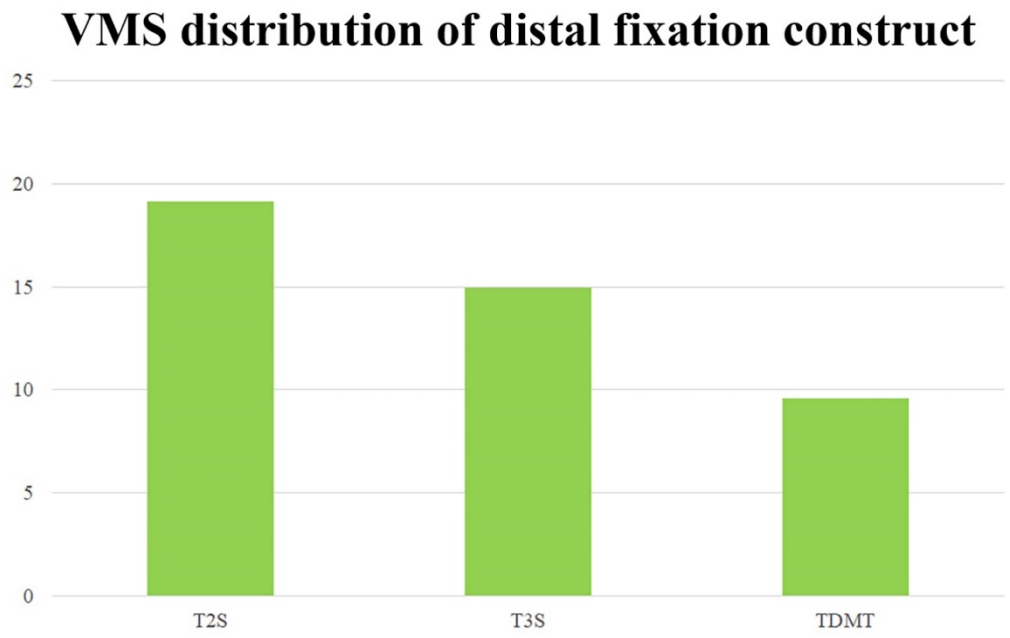

Figure 11. The VMS value of tibia in the similar area was the lowest in the plating model: (A) IMN of two-screw model (T2S), (B) IMN of three-screw model (T3S), and (C) Plating model (TDMT).

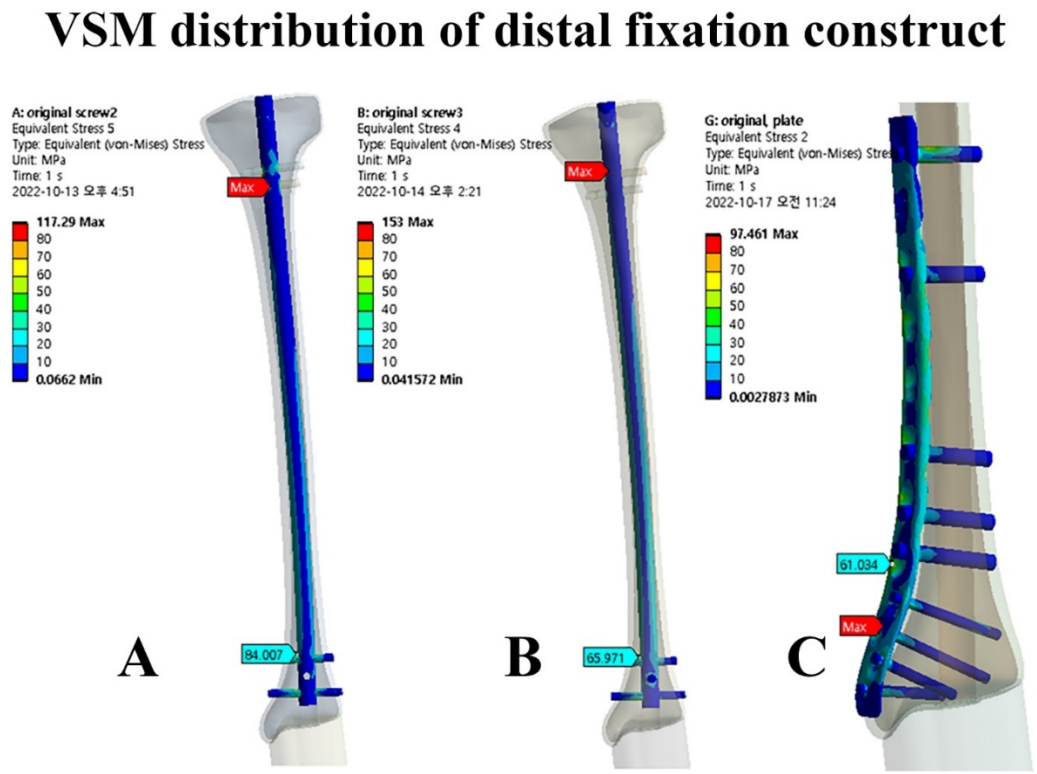

Figure 12. Stress distribution areas had the maximum VMS values at the 1st hole for the interlocking screw in IMN models and at the 3rd locking hole from the distal end in the plate model: (A) IMN of two-screw model, (B) IMN of three-screw model, and (C) Plating model.

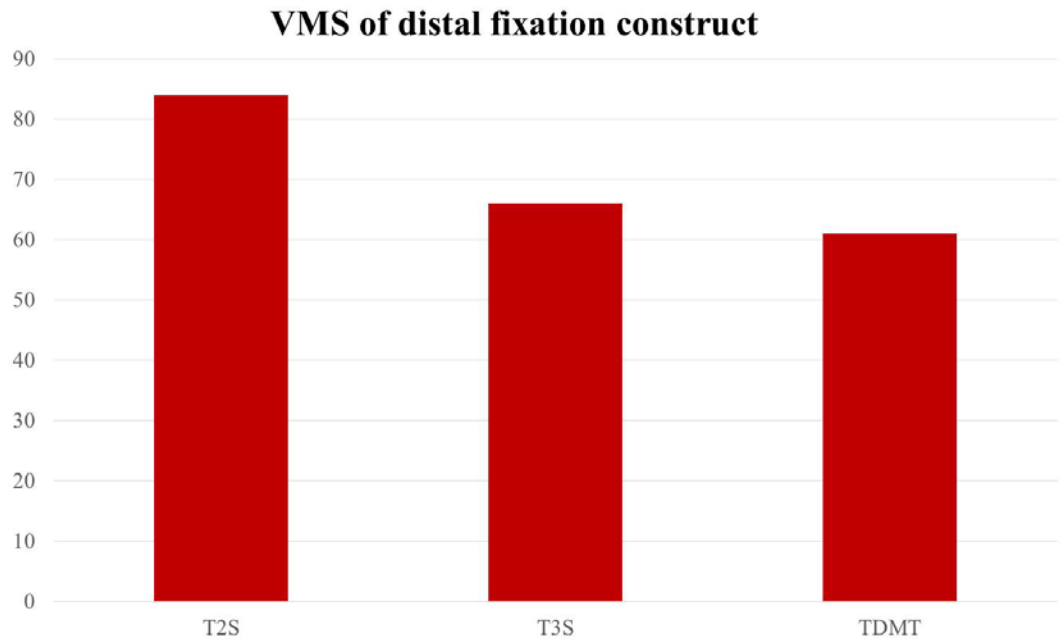

Figure 13. The VMS value of implant in the similar area was the highest in the two-screw model: (A) IMN of two-screw model (T2S), (B) IMN of three-screw model (T3S), and (C) Plating model (TDMT).

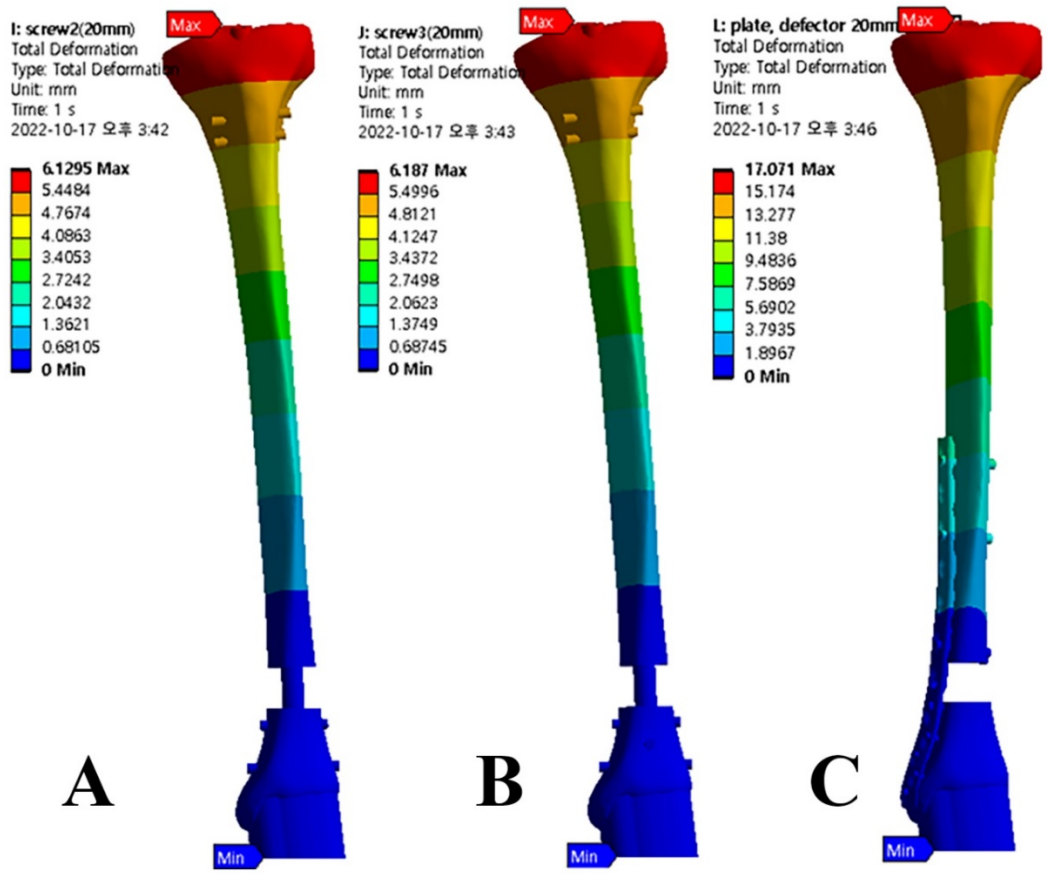

Figure 14. The assembled tibia model with 20 mm-gap indicates the maximum displacement occurring at the upper part of tibia: (A) IMN of two-screw model, (B) IMN of three-screw model, and (C) Plating model.

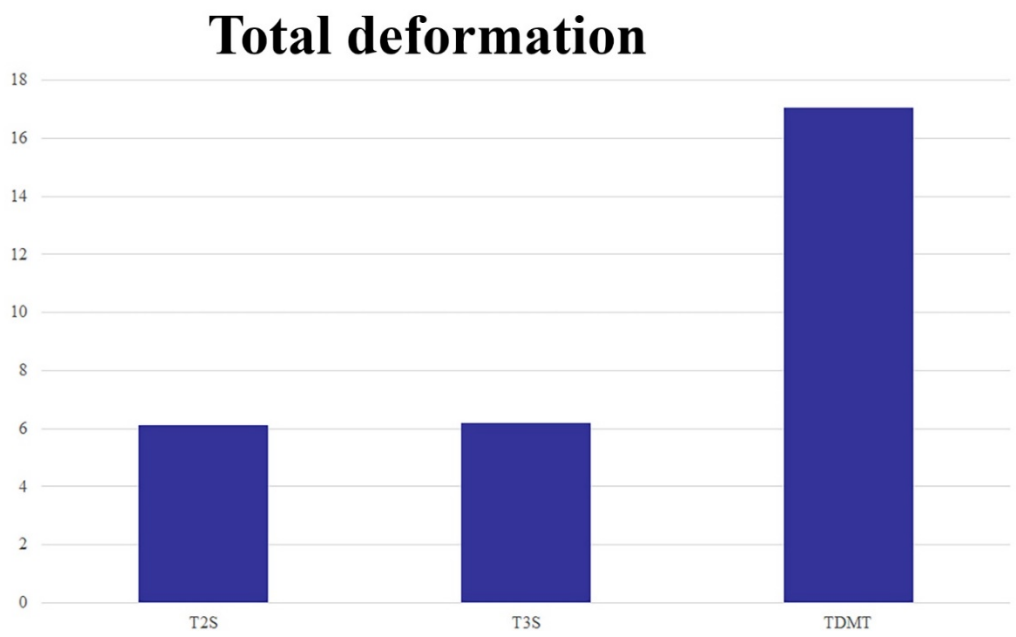

Figure 15. Total displacement was the highest in the plating model: (A) IMN of two-screw model (T2S), (B) IMN of three-screw model (T3S), and (C) Plating model (TDMT).

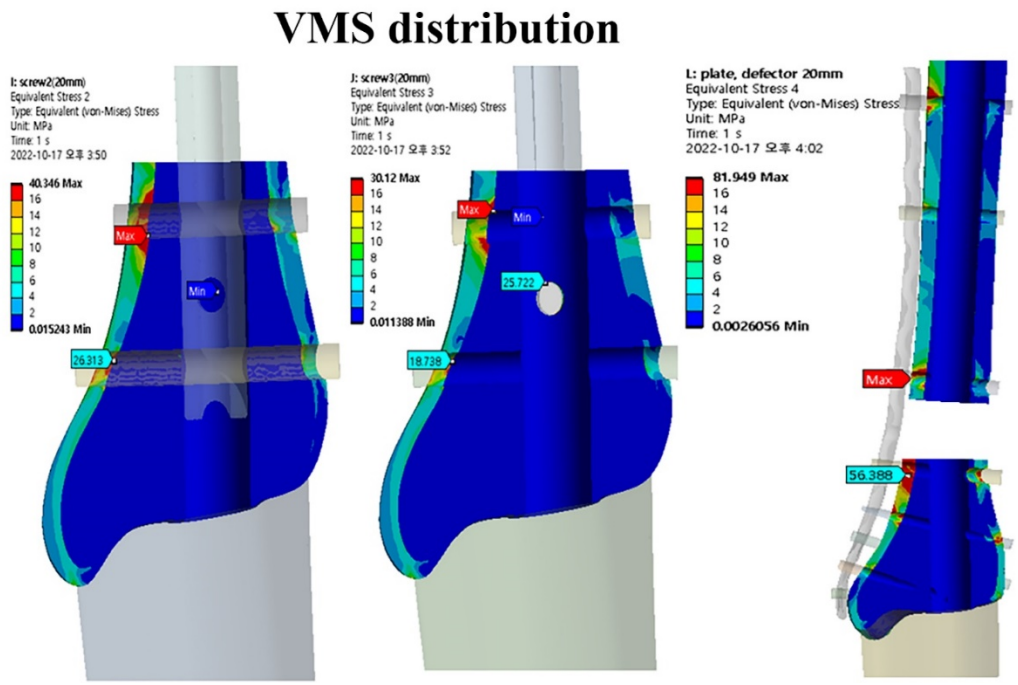

Figure 16. Stress distribution areas had the maximum VMS values at the medial cortex around 1st interlocking screw in IMN models and at the medial cortex of just the proximal hole above the fracture in the plating model.

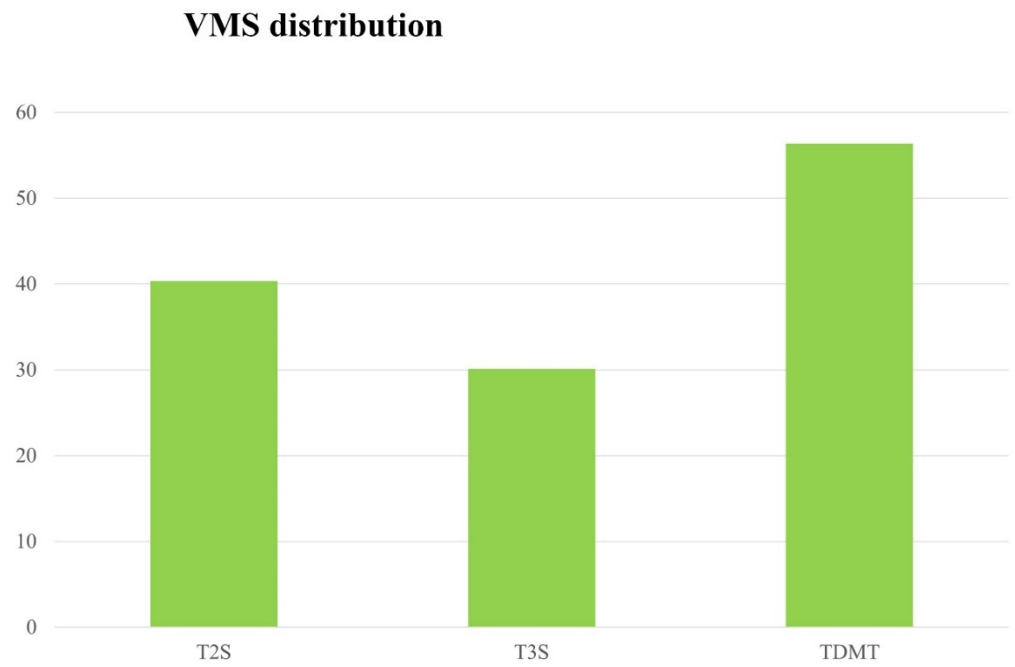

Figure 17. VMS distribution of tibia with 20 mm-gap was the highest in the plating model: (A) IMN of two-screw model (T2S), (B) IMN of three-screw model (T3S), and (C) Plating model (TDMT).

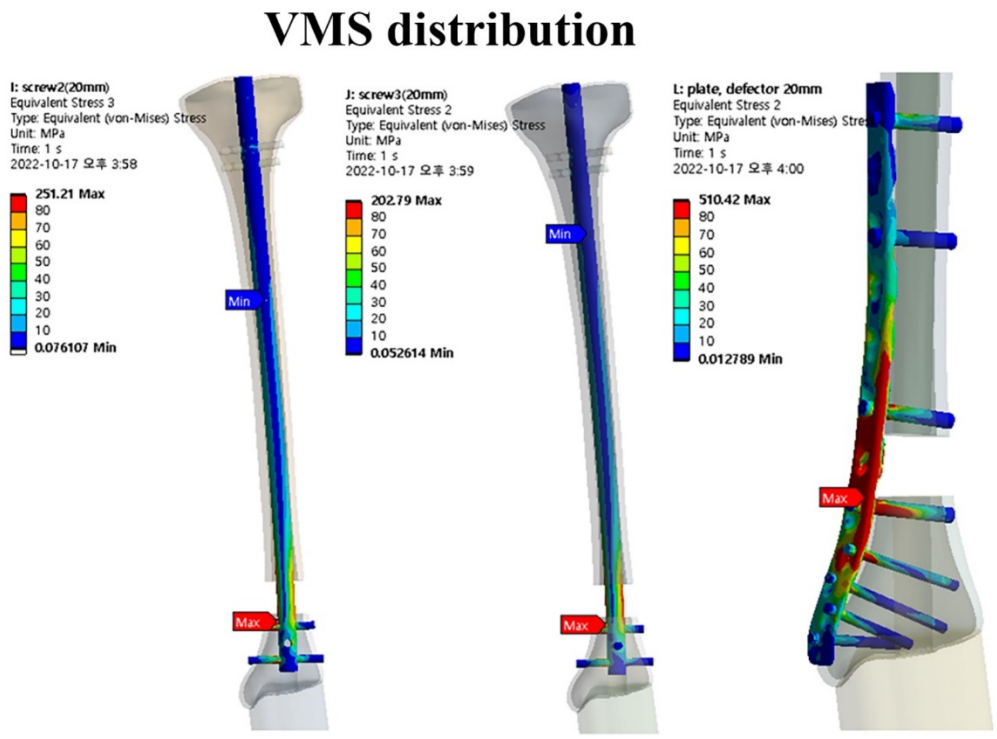

Figure 18. Stress distribution areas had the maximum VMS values at the 1st hole for the interlocking screw in IMN models and at the 5th locking hole from the distal end in the plating model.

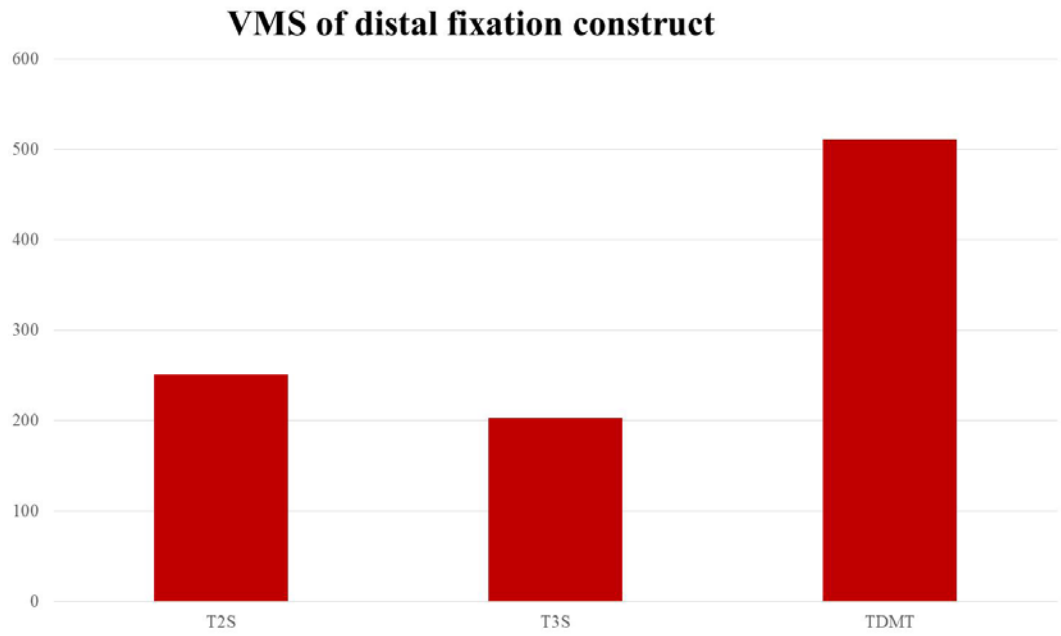

Figure 19. VMS distribution of distal fixation constructs was the highest in the plating model: (A) IMN of two-screw model (T2S), (B) IMN of three-screw model (T3S), and (C) Plating model (TDMT).

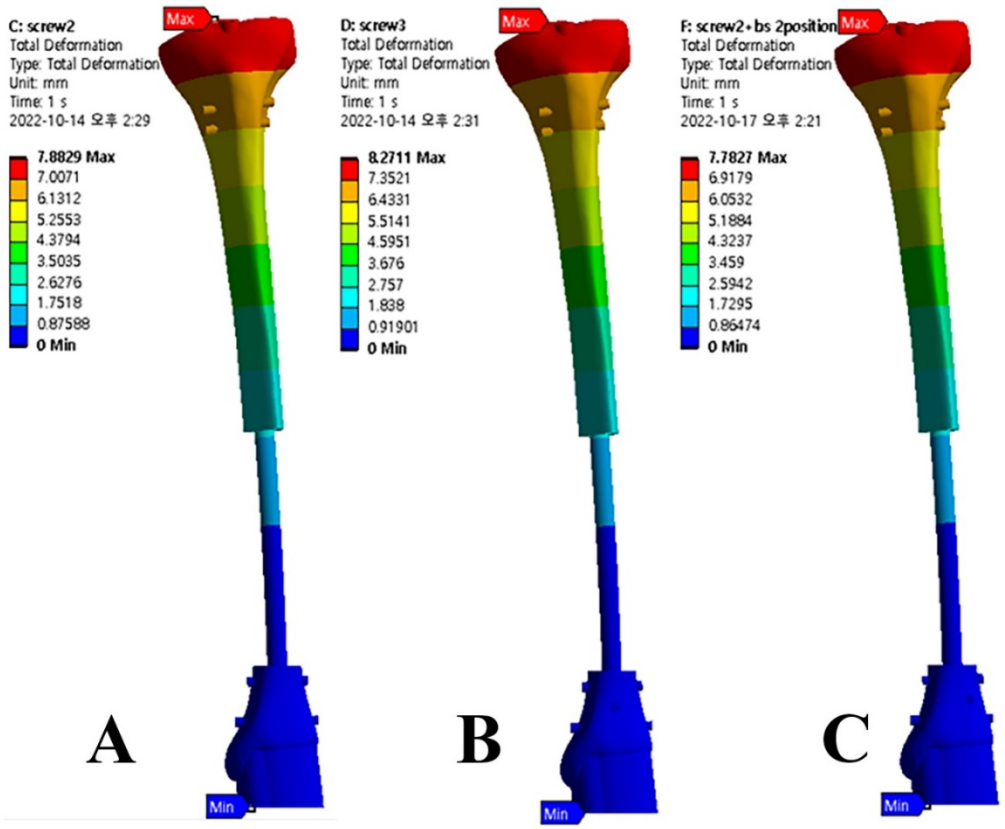

Figure 20. The assembly tibia model with 120 mm-gap indicates the maximum displacement occurring at the upper part of tibia: (A) IMN of two-screw model, (B) IMN of three-screw model, and (C) Blocking screw model.

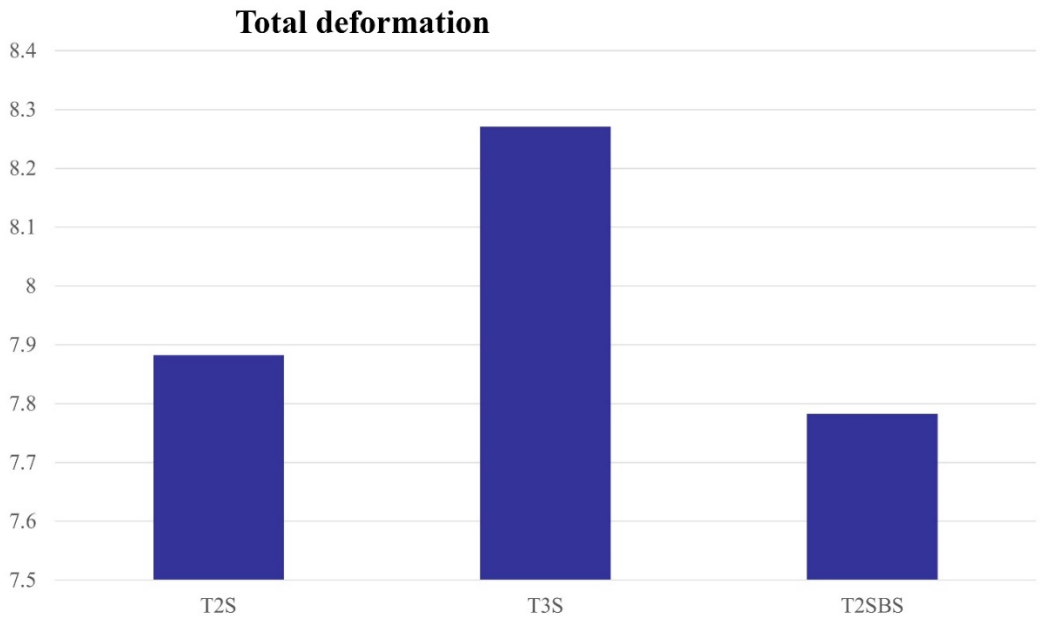

Figure 21. Total displacement was the highest in the three-screw model: (A) IMN of two-screw model, (B) IMN of three-screw model, and (C) Blocking screw model.

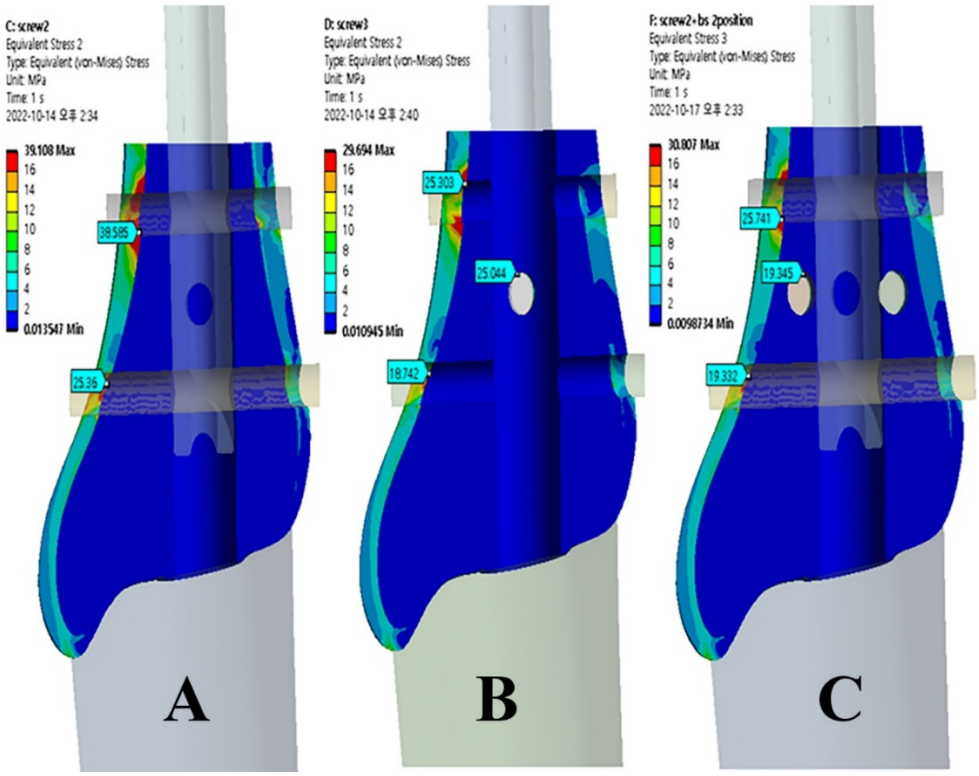

Figure 22. Stress distribution areas of tibia had the maximum VMS values around the 1st hole for the interlocking screw: (A) IMN of two-screw model, (B) IMN of three-screw model, and (C) Blocking screw model.

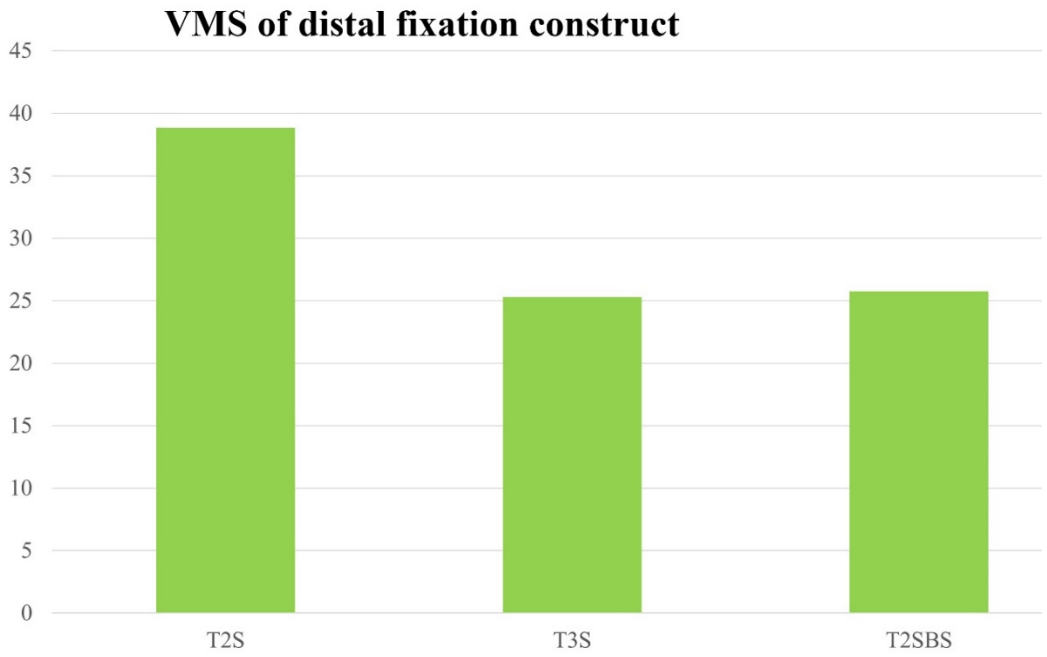

Figure 23. VMS distribution of tibia was the highest in the two-screw model: (A) IMN of two-screw model, (B) IMN of three-screw model, and (C) Blocking screw model.

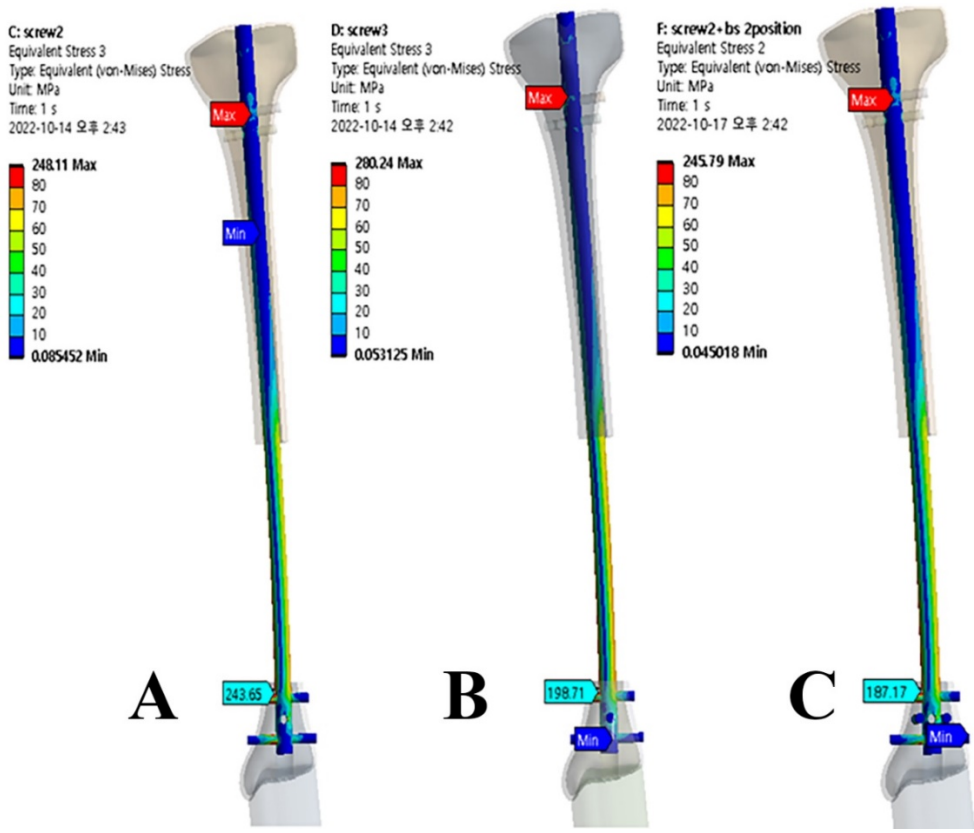

Figure 24. Stress distribution of implant had the maximum VMS values in the 1st interlocking screw hole.

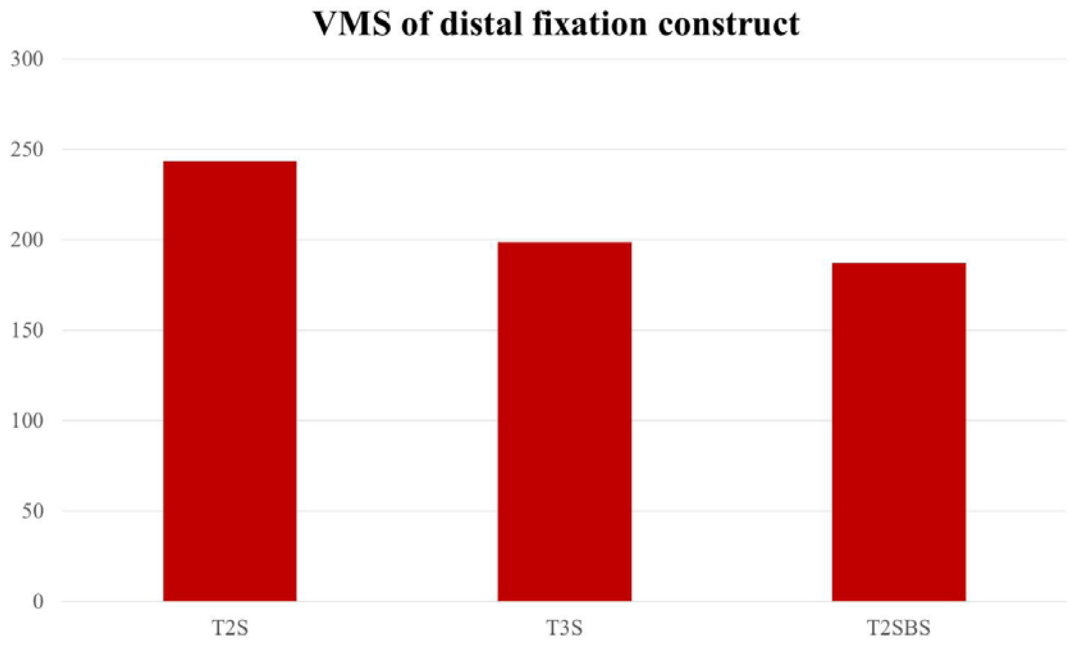

Figure 25. VMS distribution of implant was the highest in the two-screw model: (A) IMN of two-screw model, (B) IMN of three-screw model, and (C) Blocking screw model.

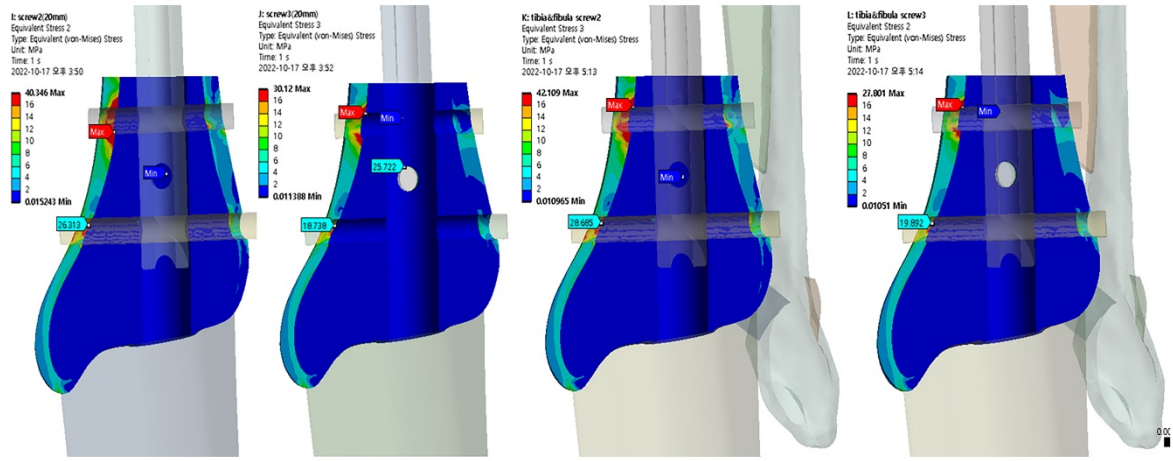

Figure 26. Assembled tibiofibular model with 20 mm-gap indicates the maximum VMS distribution in the cortex around the 1st interlocking screw hole similar to the tibia model.

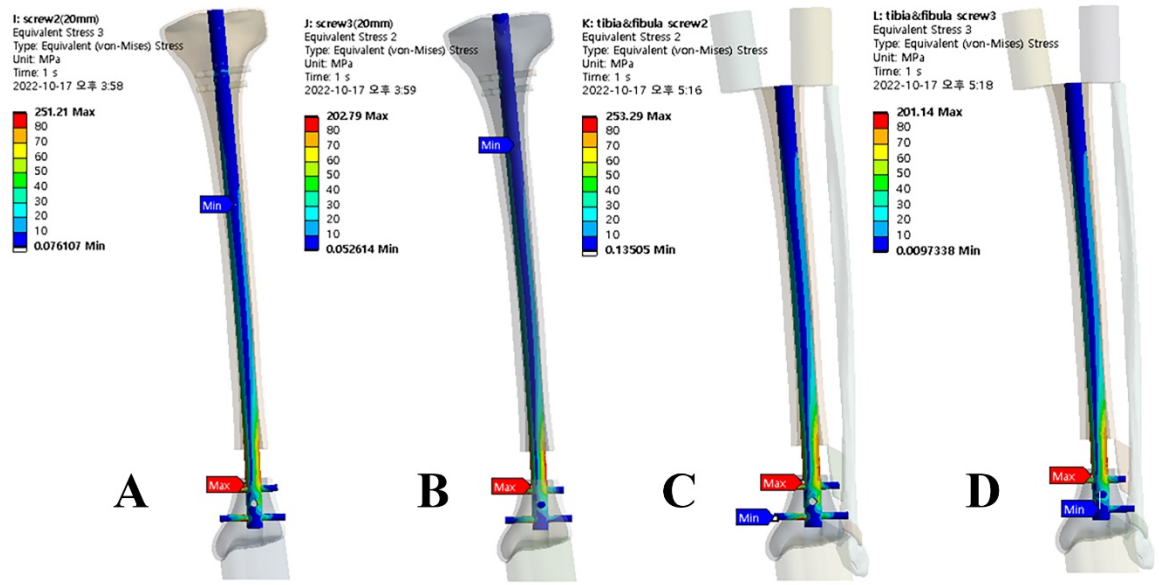

Figure 27. Assembled tibiofibular model with 20 mm-gap indicates the maximum VMS distribution in the 1st interlocking screw hole similar to the tibia model.

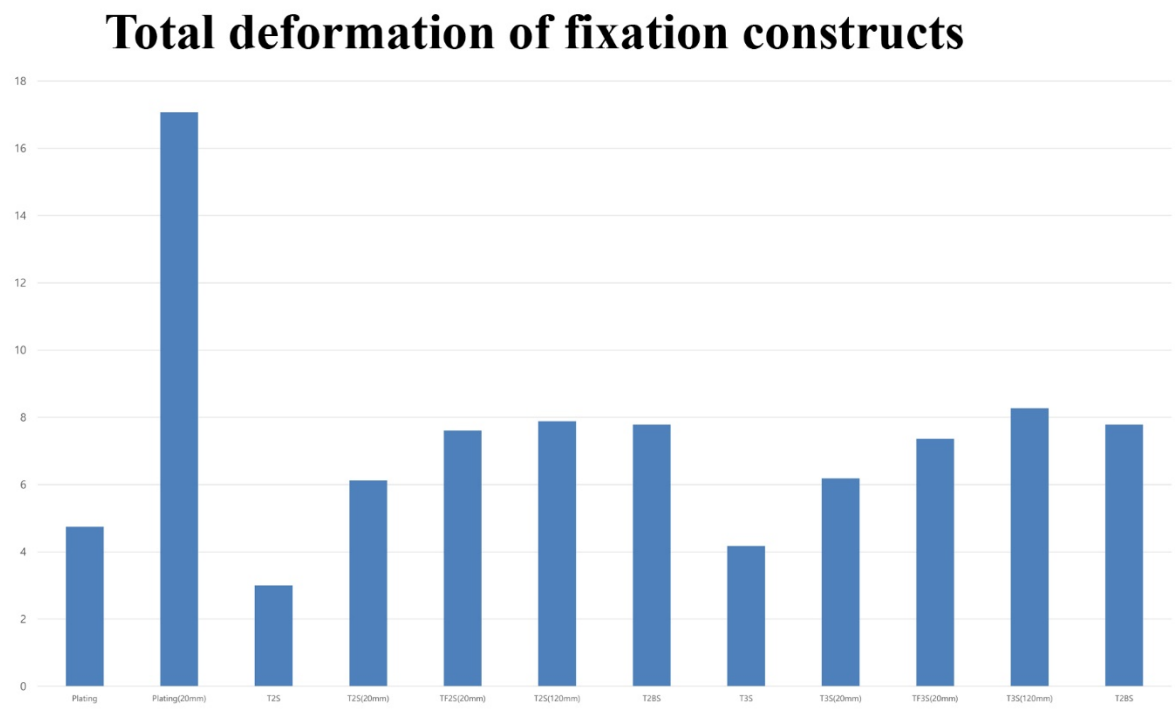

Figure 28. Total deformation of fixation construct was the highest in the plating tibia with 20mm-gap. Among fixation constructs of 120 mm-gap, the blocking screw model had the least deformation. Thus, it was stiffer than the three-screw model.

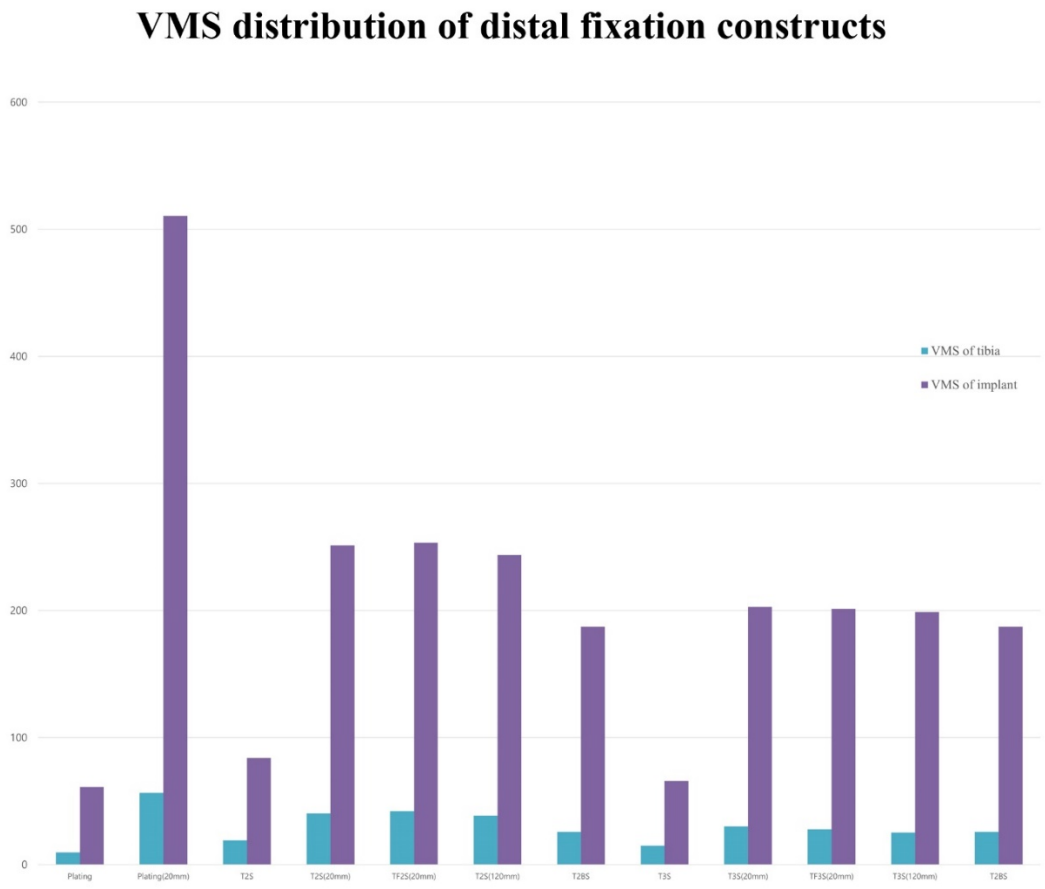

Figure 29. Among fixation constructs of 120 mm-gap, the blocking screw model had the least VMS distribution of implant. Thus, it was biomechanically more stable than the three-screw model.